

# Thermophysical Properties of the Ionic Liquids [EMIM][B(CN)<sub>4</sub>] and [HMIM][B(CN)<sub>4</sub>]

Thomas M. Koller,<sup>†</sup> Michael H. Rausch,<sup>†,‡</sup> Javier Ramos,<sup>§</sup> Peter S. Schulz,<sup>||</sup> Peter Wasserscheid,<sup>||</sup> Ioannis G. Economou,<sup>⊥,#</sup> and Andreas P. Fröba<sup>\*,†,‡</sup>

<sup>†</sup>Erlangen Graduate School in Advanced Optical Technologies, University of Erlangen-Nuremberg, Paul-Gordan-Straße 6, D-91052 Erlangen, Germany

<sup>‡</sup>Department of Chemical and Biological Engineering, Institute of Engineering Thermodynamics, University of Erlangen-Nuremberg, Am Weichselgarten 8, D-91058 Erlangen, Germany

<sup>§</sup>BIOPHYM, Departamento de Física Macromolecular, Instituto de Estructura de la Materia, CSIC, Serrano 113bis, 28006-Madrid, Spain

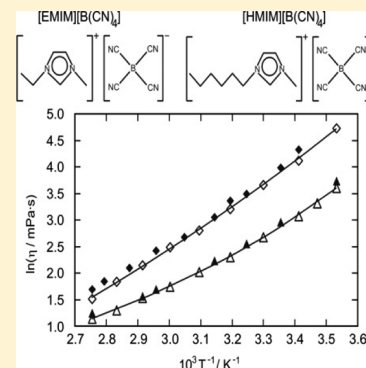
<sup>||</sup>Department of Chemical and Biological Engineering, Institute of Chemical Reaction Engineering, University of Erlangen-Nuremberg, Egerlandstraße 3, D-91058 Erlangen, Germany

<sup>⊥</sup>Molecular Thermodynamics and Modelling of Materials Laboratory, Institute of Advanced Materials, Physicochemical Processes, Nanotechnology and Microsystems, National Centre for Scientific Research "Demokritos", GR-153 10 Aghia Paraskevi Attikis, Greece

<sup>#</sup>Chemical Engineering Program, Texas A&M University at Qatar, Education City, P.O. Box 23874, Doha, Qatar

## S Supporting Information

**ABSTRACT:** In the present study, the thermophysical properties of the tetracyanoborate-based ionic liquids (ILs) 1-ethyl-3-methylimidazolium tetracyanoborate ([EMIM][B(CN)<sub>4</sub>]) and 1-hexyl-3-methylimidazolium tetracyanoborate ([HMIM][B(CN)<sub>4</sub>]) obtained by both experimental methods and molecular dynamics (MD) simulations are presented. Conventional experimental techniques were applied for the determination of refractive index, density, interfacial tension, and self-diffusion coefficients for [HMIM][B(CN)<sub>4</sub>] at atmospheric pressure in the temperature range from 283.15 to 363.15 K. In addition, surface light scattering (SLS) experiments provided accurate viscosity and interfacial tension data. As no complete molecular parametrization was available for the MD simulations of [HMIM][B(CN)<sub>4</sub>], our recently developed united-atom force field for [EMIM][B(CN)<sub>4</sub>] was partially transferred to the homologous IL [HMIM][B(CN)<sub>4</sub>]. Deviations between our simulated and experimental data for the equilibrium properties are less than  $\pm 0.3\%$  in the case of density and less than  $\pm 8\%$  in the case of interfacial tension for both ILs. Furthermore, the calculated and measured data for the transport properties viscosity and self-diffusion coefficient are in good agreement, with deviations of less than  $\pm 30\%$  over the whole temperature range. In addition to a comparison with the literature, the influence of varying cation chain length on thermophysical properties of [EMIM][B(CN)<sub>4</sub>] and [HMIM][B(CN)<sub>4</sub>] is discussed.



## INTRODUCTION

Ionic liquids (ILs) are low-temperature molten salts and have attracted a rapidly increasing interest during the past several years, at both the academic and industrial level.<sup>1</sup> Because of their unique properties of being liquid over a wide temperature range, being nearly nonvolatile and nonflammable, and exhibiting an excellent dissolving power for a wide range of inorganic and organic materials, ILs are potential working fluids in diverse technical fields.<sup>2</sup> In this respect, these fluids can be tailored to specific applications because of the almost unlimited number of potential combinations of cations and anions forming an IL. Yet, knowledge about the resulting thermophysical properties is crucial for the optimum design of processes and plants in engineering. Naturally, these properties cannot be measured for

every conceivable IL as this would require an enormous effort in time and resources.<sup>2</sup>

Thanks to increasing computational capabilities, theoretical models or accurate computational approaches are useful alternatives to overcome experimental limitations. One of these methods gaining interest in the scientific and industrial community is molecular dynamics (MD) simulation, which is a reliable instrument for understanding the structure–property relationships and rational design of new ILs. In addition, MD has turned out to be a very useful tool for predicting equilibrium and transport properties of ILs.<sup>1,3</sup> Nevertheless, MD simulation is

Received: January 10, 2013

Revised: June 18, 2013

Published: June 21, 2013

subject to the same restriction as all prediction methods and can only be as accurate as the experimental data used for the development of force fields (FFs).

To determine how reliably MD simulation can predict the thermophysical properties of ILs, simulation results for 1-ethyl-3-methylimidazolium tetracyanoborate ([EMIM][B(CN)<sub>4</sub>]) were compared to experimental data in our previous studies.<sup>4,5</sup> Because of its attractive properties, such as very low viscosity, high electric conductivity, and high chemical and thermal stability,<sup>5–8</sup> this IL is considered for use as an electrolyte in dye-sensitized solar cells<sup>9,10</sup> or as a solvent for the separation of CO<sub>2</sub> from N<sub>2</sub>,<sup>11</sup> for example. Accurate experimental data for [EMIM][B(CN)<sub>4</sub>] were obtained from a comprehensive study of the IL using conventional methods and the surface light scattering (SLS) technique.<sup>5</sup> These data were used for the development of a molecular FF of the IL and finally for a validation of the MD simulations performed.<sup>4</sup> A comparison between the simulated and experimental results revealed good agreement for density, with deviations of less than  $\pm 0.3\%$ , and for the transport properties viscosity and self-diffusion coefficient, with deviations of less than  $\pm 20\%$ .<sup>4</sup>

In this work, a combined experimental and molecular simulation study of the IL 1-hexyl-3-methylimidazolium tetracyanoborate ([HMIM][B(CN)<sub>4</sub>]) was carried out regarding thermophysical properties. The nonelectrostatic FF developed for [EMIM][B(CN)<sub>4</sub>] was transferred consistently to the longer-chain homologous IL [HMIM][B(CN)<sub>4</sub>]. To identify how reliably different thermophysical properties can be calculated with the transferred molecular FF, properties such as density, self-diffusion coefficients, and viscosity were investigated in accordance with our studies performed for [EMIM][B(CN)<sub>4</sub>].<sup>4,5</sup> Furthermore, the interfacial tension was simulated for [EMIM][B(CN)<sub>4</sub>] and [HMIM][B(CN)<sub>4</sub>]. The influence of the alkyl-chain length and intermolecular interactions on the thermophysical properties of both ILs is discussed. Finally, the experimental data obtained for [HMIM][B(CN)<sub>4</sub>] in the present study are compared to available literature data.

## ■ EXPERIMENTAL SECTION

In this section, only the essential information for the sample preparation of [HMIM][B(CN)<sub>4</sub>] and the experimental techniques used for the determination of its refractive index, density, self-diffusion coefficients, viscosity, and interfacial tension is given. For a detailed description of the fundamentals and experimental realization of the techniques employed, especially in relation to their application to ILs, the reader is referred to the literature.<sup>5,12–20</sup>

The IL [HMIM][B(CN)<sub>4</sub>] (molecular weight  $M = 282.16$  g·mol<sup>−1</sup>) was provided by Merck KGaA, Darmstadt, Germany. Its nominal purity was verified by <sup>1</sup>H NMR analysis (JEOL, ECX-400 spectrometer) to be higher than 99%. The concentration of water was determined by Karl Fischer coulometric titration (Metrohm, 756 KF coulometer) after the sample preparation procedure and after the SLS experiments. The expanded uncertainty on a confidence level of more than 95% ( $k = 2$ ) of the water content measurements yielding average values of 387 ppm before and 456 ppm after the experiments is estimated to be less than  $\pm 20\%$ .

The refractive index,  $n_D$ , at the sodium line ( $\lambda_D = 589.3$  nm) and the refractive index difference,  $n_F - n_C$ , for the Fraunhofer lines ( $\lambda_F = 486.1$  nm and  $\lambda_C = 656.3$  nm) were measured with an Abbe refractometer (Leo Kuebler, R 6000 G) at which the sample temperature was controlled to within  $\pm 0.02$  K and

measured with an absolute uncertainty of  $\pm 0.5$  K. The expanded uncertainties ( $k = 2$ ) in the measurement of the refractive index and the refractive index difference of [HMIM][B(CN)<sub>4</sub>] are estimated to be less than  $\pm 0.0005$  and  $\pm 0.001$ , respectively.

Measurements of the density  $\rho$  at atmospheric pressure are based on the vibrating-tube method (Anton Paar, DMA 5000). The temperature of the U-tube was controlled within  $\pm 1$  mK and measured by a high-precision platinum resistance probe with an uncertainty of  $\pm 10$  mK. The expanded uncertainty ( $k = 2$ ) of the present density measurements for the IL [HMIM][B(CN)<sub>4</sub>] is estimated to be less than  $\pm 0.02\%$ .

The self-diffusion coefficients  $D_{\pm}$  of the cation and anion were derived from pulsed-field gradient spin-echo NMR measurements using the <sup>1</sup>H nuclei in the methyl and hexyl groups of the cation and the <sup>11</sup>B nucleus in the anion. A bipolar pulse longitudinal eddy current delay was applied as pulse sequence with a sine gradient shape. The temperature stability during the experiments was better than  $\pm 0.5$  K, and the absolute uncertainty in the temperature measurement was  $\pm 0.05$  K. The expanded uncertainty ( $k = 2$ ) of the NMR experimental data is estimated to be less than  $\pm 10\%$ .

Measurements of the interfacial tension  $\sigma$  using the pendant drop technique (OEG, SURFTENS universal) were performed at a single temperature of  $295.15 \pm 0.1$  K inside an optical glass cell for photometry (Hellma, 402.000) under an argon atmosphere. For the interfacial tension datum at 295.15 K, the expanded uncertainty ( $k = 2$ ) is estimated to be less than  $\pm 1\%$ . In the temperature range from 283.15 to 333.15 K, the interfacial tension  $\sigma$  was predicted by

$$\sigma = \sigma_{\text{ref}}(\rho/\rho_{\text{ref}})^4 \quad (1)$$

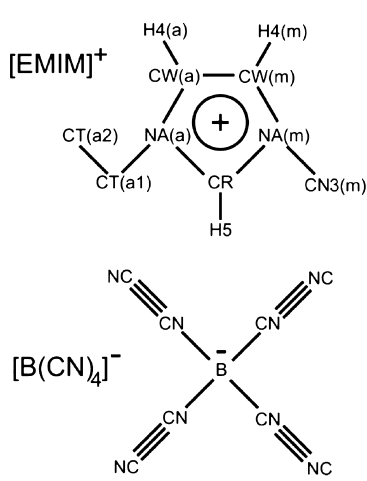
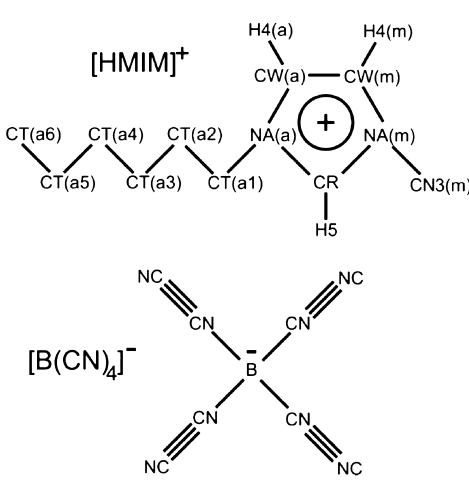
where  $\sigma_{\text{ref}}$  and  $\rho_{\text{ref}}$  are the measured interfacial tension and density, respectively, at the reference temperature of 295.15 K (cf. refs 20 and 21). The proposed scheme predicts the interfacial tension of high-viscosity fluids with a typical uncertainty of less than 2% tested for several reference fluids (see, e.g., ref 22).

For temperatures between 283.15 and 333.15 K, at a first approximation, SLS could provide access to only the ratio of the interfacial tension  $\sigma$  to the dynamic viscosity,  $\eta$ , of [HMIM][B(CN)<sub>4</sub>]. Here, the evaluation of the dynamic viscosity was based on the combination of the SLS technique and the pendant drop method. For temperatures of 343.15, 353.15, and 363.15 K, the interfacial tension and viscosity of [HMIM][B(CN)<sub>4</sub>] could be determined simultaneously by SLS. In both cases, data for the viscosity and interfacial tension were obtained by an exact numerical solution of the dispersion equation for a free liquid surface. The expanded uncertainty ( $k = 2$ ) for the dynamic viscosity,  $\eta$ , for temperatures between 283.15 and 333.15 K is estimated to be less than  $\pm 3\%$ . For higher temperatures, the expanded uncertainties ( $k = 2$ ) for the dynamic viscosity and the interfacial tension  $\sigma$  are estimated to be less than  $\pm 6\%$  and less than  $\pm 8\%$ , respectively. The relatively large uncertainties are caused by the experimental complexity in the region where the surface fluctuations studied by SLS change between overdamped and oscillatory behavior.

## ■ MOLECULAR DYNAMICS (MD) SIMULATION

The reliability of the prediction of thermophysical properties by MD simulation is inevitably associated with the accuracy of the atomistic FF. For [EMIM][B(CN)<sub>4</sub>], we developed a non-polarizable united-atom (UA) FF with the requirement of being computationally low-demanding and effective.<sup>4</sup> This FF is

Table 1. Comparison of Partial Charges  $q_i$  (in Units of  $e$ ) for Each Atom  $i$  of [EMIM][B(CN)<sub>4</sub>]<sup>a</sup> and [HMIM][B(CN)<sub>4</sub>] Obtained from Quantum Calculations

atom	$q_i / e$	
		
	cation	
CR	-0.0124	-0.0050
NA(m)	-0.0352	-0.0414
NA(a)	-0.0205	-0.0755
CW(m)	-0.1705	-0.1890
CW(a)	-0.2067	-0.1412
H5	0.2276	0.2201
H4(m)	0.2382	0.2451
H4(a)	0.2555	0.2287
CN3(m)	0.2832	0.2860
CT(a1)	0.2524	0.2742
CT(a2)	0.0391	0.0198
CT(a3)	-	0.0198
CT(a4)	-	0.0098
CT(a5)	-	0.0000
CT(a6)	-	0.0000
TOTAL	0.8426	0.8514
	anion	
B	0.3511	0.3386
CN	0.1303	0.1406
NC	-0.4287	-0.4381
TOTAL	-0.8426	-0.8514

<sup>a</sup>Taken from our Previous Study.<sup>4</sup>

characterized by a potential energy function in terms of electrostatic and nonelectrostatic interactions. Regarding the details of the molecular FF and the simulation methodology for [EMIM][B(CN)<sub>4</sub>], the reader is referred to our previous study.<sup>4</sup> In the present study, we applied the corresponding procedures for [HMIM][B(CN)<sub>4</sub>] in a similar manner. In this section, the

relevant information and modifications compared to [EMIM]-[B(CN)<sub>4</sub>] are given in detail.

In the case of the electrostatic FF, quantum calculations for [HMIM][B(CN)<sub>4</sub>] were necessary because the effect of the longer alkyl chain could influence the partial charges, particularly those of the imidazolium ring. Because of the extremely time-

consuming calculations required for [HMIM][B(CN)<sub>4</sub>] originating from the increasing number of dihedral conformations in the alkyl chain of the cation, we decided to analyze 1-butyl-3-methylimidazolium tetracyanoborate ([BMIM][B(CN)<sub>4</sub>]), with an alkyl-chain length between those of the [EMIM]<sup>+</sup> and [HMIM]<sup>+</sup> cations, as an approximation. For [BMIM][B(CN)<sub>4</sub>], 216 × 3 different initial ionic-pair conformations were built. Here, the number 3 denotes three different positions of the [B(CN)<sub>4</sub>]<sup>−</sup> anion with respect to the [BMIM]<sup>+</sup> cation. These positions were chosen similarly to the energetically preferable positions found for [EMIM][B(CN)<sub>4</sub>] from our quantum calculations.<sup>4</sup> The use of these geometrical structures as input data served to accelerate the calculations performed at the MP2/6-31G\*+ level. The other number, 216, reflects the different conformations of three dihedral angles of the butyl chain in the [BMIM]<sup>+</sup> cation taking into account six different angles from 0° to 300° with a step of 60°. Hence, 6<sup>3</sup> = 216 conformers are obtained for the [BMIM]<sup>+</sup> cation, whereas 6<sup>5</sup> = 7776 conformers would have to be considered for the [HMIM]<sup>+</sup> cation. For the 25 most stable ionic-pair configurations obtained from the quantum calculations at the MP2/6-31G\*+ level, the ensemble-average restrained electrostatic potential (EA-RESP) method was applied for computing the charges of [BMIM][B(CN)<sub>4</sub>]. These charges were directly used as charges for [HMIM][B(CN)<sub>4</sub>]. For the two additional UAs in the hexyl chain of the [HMIM]<sup>+</sup> cation, the partial charges were assumed to be equal to 0. This assumption seems to be straightforward, as the electrostatic potential is expected to decrease strongly for longer alkyl chains, which is confirmed within our calculations. The atomistic charges calculated by the EA-RESP method taking into account the most stable ionic-pair configurations are given for [EMIM][B(CN)<sub>4</sub>] and [HMIM][B(CN)<sub>4</sub>] in Table 1.

With the EA-RESP method, the total charges for the cation and anion of [HMIM][B(CN)<sub>4</sub>] were reduced from ±e to ±0.85e, which is very close to the charges of ±0.84e for [EMIM][B(CN)<sub>4</sub>]. This reduction automatically results from the charge procedure averaged over all stable configurations without any manual rescaling of the atomistic charges. Comparing the individual charges for [HMIM][B(CN)<sub>4</sub>] with those for [EMIM][B(CN)<sub>4</sub>], deviations can mainly be found for the atoms in the aromatic ring of the cations. The charge of the NA(a) atom located next to the alkyl chain is more negative in [HMIM]<sup>+</sup> than in [EMIM]<sup>+</sup>. Thus, the NA(a) atom seems to attract electrons from the longer alkyl chain in [HMIM]<sup>+</sup> more strongly than in [EMIM]<sup>+</sup>. Because of the stronger electronegativity of the NA(a) atom in the [HMIM]<sup>+</sup> cation, the charges of the linked CW(a), CR, and CT(a1) atoms are more positive. In the [B(CN)<sub>4</sub>]<sup>−</sup> anion of both ILs, the observable electrostatic differences related to an increasing charge separation or polarity in the CN–NC bonds for [HMIM][B(CN)<sub>4</sub>] might result from the interaction with the cations. In conclusion, the different charge distributions in both ions of the two ILs demonstrate that the computations performed for the electrostatic FF were essential for a reasonable calculation of the partial charges for [HMIM][B(CN)<sub>4</sub>].

For the implementation of the nonelectrostatic FF of [HMIM][B(CN)<sub>4</sub>], the optimized parameter set used for the MD simulations with [EMIM][B(CN)<sub>4</sub>] was transferred.<sup>4</sup> The additional UAs for the hexyl chain in the [HMIM]<sup>+</sup> cation were treated according to the method of Liu et al.,<sup>23</sup> who used the AMBER FF.<sup>24</sup> Regarding the anion, only the Lennard-Jones (LJ) size parameter of the nitrogen atoms in the anion was shifted

from 0.32 to 0.33 nm to adjust the simulated to the experimental density of [HMIM][B(CN)<sub>4</sub>] at a temperature of 298.15 K.

The computational methods and the evaluation techniques for density, self-diffusion coefficients, and viscosity of [HMIM][B(CN)<sub>4</sub>] are identical to those used for our investigations of [EMIM][B(CN)<sub>4</sub>] and are only summarized briefly here. More details are given on the evaluation procedure for the interfacial tension, which was used for both ILs in the present study. The GROMACS 4.0.7 simulation package<sup>25</sup> was used for all simulations reported here. The Nosé–Hoover thermostat<sup>26,27</sup> and Parrinello–Rahman barostat<sup>28,29</sup> with coupling times of  $\tau_T = 0.03$  ps and  $\tau_p = 0.7$  ps, respectively, were used to control temperature and pressure conditions. For the Coulombic and LJ interactions, the cutoff was set to 1.2 nm. The full electrostatic interactions were considered by the particle mesh Ewald (PME) summation,<sup>30</sup> whereas classical long-range LJ corrections for the dispersion term were considered for energy and pressure.<sup>25</sup> A time step of 2 fs was used, employing periodic boundary conditions in all directions. MD simulations for the IL [HMIM][B(CN)<sub>4</sub>] were performed at a pressure of 1 bar over a temperature range from 283.15 to 393.15 K. The simulated systems were composed of 50 ion pairs, equal to 1200 atoms in a simulation box. At first, four different initial configurations of [HMIM][B(CN)<sub>4</sub>] obtained from the quantum calculations were energetically minimized using the conjugate gradient energy minimization for each temperature and equilibrated for a period of 2 ns in the NVT and NPT ensembles. Thereafter, NPT simulations on the order of 5 ns were performed, from which the mass density  $\rho$  was extracted. From the equilibrated structures at the calculated density, the self-diffusion coefficients for the cation ( $D_+$ ) and the anion ( $D_-$ ) were computed from NVT runs on the order of 10 ns based on the mean square displacement (MSD) of each ion according to the Einstein equation.<sup>31</sup> In accordance with our previous simulation study<sup>4</sup> for [EMIM][B(CN)<sub>4</sub>], the coefficient  $\beta = d[\log(\text{MSD})]/d[\log(t)]$  was used to characterize the linear Fickian diffusive regime ( $\beta = 1$ ). In Figure S1 of the Supporting Information, double-logarithmic plots for the MSD as a function of the simulation time  $t$  are shown for both ions of [HMIM][B(CN)<sub>4</sub>] at temperatures of 293.15 and 318.15 K, as examples. For a reliable analysis, the self-diffusion coefficients were obtained from the linear parts of the corresponding function where  $\beta$  approaches the value of 1. For calculations of the dynamic viscosity,  $\eta$ , with the equilibrium Green–Kubo method,<sup>31</sup> the simulation time in the NVT ensemble was extended to 30 ns. The data for the viscosity were obtained from the plateaus of the corresponding integrated pressure autocorrelation function of the off-diagonal elements of the stress tensor.

For the computation of the interfacial tension  $\sigma$ , a common simulation method based on the analysis of the virial pressure tensor was tested. Here, the interfacial tension was calculated from the simulation-time- ( $t$ -) dependent evolution of the diagonal elements of the pressure tensor  $p_{ii}$  according to<sup>32–35</sup>

$$\sigma = \frac{L_z}{2} \left\langle p_{zz}(t) - \frac{p_{xx}(t) + p_{yy}(t)}{2} \right\rangle \quad (2)$$

For this calculation, the equilibrated NPT ensembles of the IL were treated as slabs oriented parallel to the  $xy$  plane, with each slab having a width of about 2.8 nm located between two vacuum regions. In agreement with Bhargava and Balasubramanian,<sup>32</sup> the total length of the orthorhombic cell in the  $z$  direction,  $L_z$ , was set to 6 nm, which is more than twice as large as the lengths in the  $x$



and  $y$  directions. This length turned out to be long enough to avoid interactions between the liquid layers in the  $z$  direction. The constraint for zero vapor density can be applied in our models because ILs exhibit very small vapor pressures, especially for the relatively low temperatures studied here. After equilibration of the system over 1 ns, average values for the interfacial tensions of [EMIM][B(CN)<sub>4</sub>] and [HMIM][B(CN)<sub>4</sub>] were collected over an analysis run of about 10 ns, with the pressure tensors stored every 10 fs. Long-range corrections to energy and pressure were used assuming homogeneous conditions as an approximation. However, the relatively long cutoff of 1.2 nm, which is more than 3 times the largest LJ size parameter in the IL models and close to the limit of one-half of the box size, was assumed to consider the long-range interactions sufficiently. These issues are discussed in more detail in context with the results for the interfacial tension.

For all simulated properties, the statistical uncertainties given in the corresponding tables and figures represent twice the standard deviation of four independent runs with different initial configurations.

## RESULTS AND DISCUSSION

Different thermophysical properties of the IL [HMIM][B(CN)<sub>4</sub>] were investigated by experimental and MD simulation methods. In particular, the results for refractive index, density, interfacial tension, self-diffusion coefficients, and dynamic viscosity are discussed. In the corresponding subsections, the experimental results for [HMIM][B(CN)<sub>4</sub>] are presented first. Then, the simulation results are compared to the experimental data for [HMIM][B(CN)<sub>4</sub>] and the results from the previous studies<sup>4,5</sup> for [EMIM][B(CN)<sub>4</sub>]. This allows for an interpretation of the thermophysical properties in terms of structural and intermolecular effects for the homologous ILs. Thereafter, the properties for [HMIM][B(CN)<sub>4</sub>] are compared to available literature data.

**Refractive Index.** The measured data for the refractive index,  $n_D$ , and the refractive index difference,  $n_F - n_C$ , for [HMIM][B(CN)<sub>4</sub>] in the temperature range from 283.15 to 313.15 K at atmospheric pressure are summarized in Table 2 and Figure 1. In the latter, the refractive index data obtained for our measurements of [EMIM][B(CN)<sub>4</sub>] are included for comparison.

**Table 2. Experimental Values of Refractive Index,  $n_D$ , and Refractive Index Difference,  $n_F - n_C$ , for [HMIM][B(CN)<sub>4</sub>] at Atmospheric Pressure**

$T$ (K)	$n_D$	$n_F - n_C$
283.15	1.4585	0.0096
293.15	1.4548	0.0094
303.15	1.4513	0.0093
313.15	1.4477	0.0091

As can generally be observed for fluids, the refractive index decreases linearly with increasing temperature. For the limited temperature range investigated in this study, the dependence of the refractive index,  $n$ , on temperature and wavelength at atmospheric pressure can be represented well by the linear equation

$$n = n_0 + n_1 T + \frac{\Delta n}{\Delta \lambda} (\lambda - \lambda_D) \quad (3)$$

where  $T$  is the temperature in Kelvin,  $\lambda$  is the wavelength in meters, and  $\lambda_D$  ( $= 589.3 \times 10^{-9}$  m) is the wavelength at the

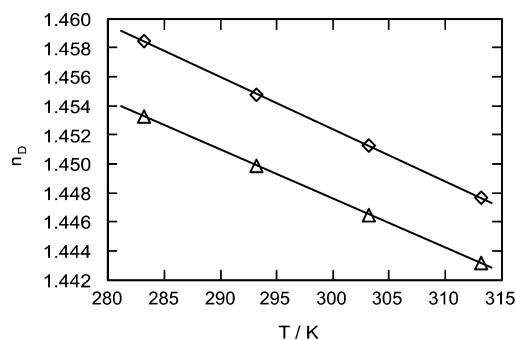


**Figure 1.** Experimental values for the refractive index,  $n_D$ , at atmospheric pressure as a function of temperature (—, eq 3): ◇, [HMIM][B(CN)<sub>4</sub>]; Δ, [EMIM][B(CN)<sub>4</sub>].<sup>5</sup>

sodium vapor line. The fit parameters in eq 3 considering the present results for [HMIM][B(CN)<sub>4</sub>] are  $n_0 = 1.56011$  and  $n_1 = -0.000359 \text{ K}^{-1}$ , and the mean dispersion is  $\Delta n / \Delta \lambda = -54777 \text{ m}^{-1}$ . The latter corresponds to the average value of the refractive index difference,  $n_F - n_C$ , related to  $\lambda_F - \lambda_C$  and is assumed to be independent of the temperature. For [HMIM][B(CN)<sub>4</sub>], the root-mean-square deviation of the experimental refractive index data from their correlation according to eq 3 is 0.004%. In addition, the deviations of the single data points from the fit are clearly within the measurement uncertainty of  $\pm 0.0005$ .

Figure 1 shows that the values of the experimental refractive index,  $n_D$ , for [HMIM][B(CN)<sub>4</sub>] are larger than those for [EMIM][B(CN)<sub>4</sub>], ranging from +0.0052 at 283.15 K to +0.0045 at 313.15 K. This behavior is consistent with the observations in our previous studies for ILs with varied cationic chain lengths.<sup>13,15</sup> According to Brocos et al.<sup>36</sup> and Deetlefs et al.,<sup>37</sup> an increasing refractive index should be found for a decreasing reduced molar free volume, that is, for a decreasing unoccupied part of the molar volume. Within our studies for imidazolium-based ILs with varying alkyl-chain lengths, however, increased refractive indices were always associated with decreasing mass densities, which seems to be in conflict with the preceding statement. It must be taken into account that further characteristics of the studied systems other than the mass density might affect the refractive index. To our knowledge, no experimental values for the refractive index for tetracyanoborate-based ILs can be found in the literature at present.

**Density.** Our experimental and simulated density data for [HMIM][B(CN)<sub>4</sub>] obtained for temperatures between 283.15 and 363.15 K are summarized in Table 3 and Figure 2. The latter also includes our density data for [EMIM][B(CN)<sub>4</sub>] obtained from experiment and simulation.<sup>4,5</sup>

The experimental density is represented well by the following polynomial of second order with respect to the temperature  $T$

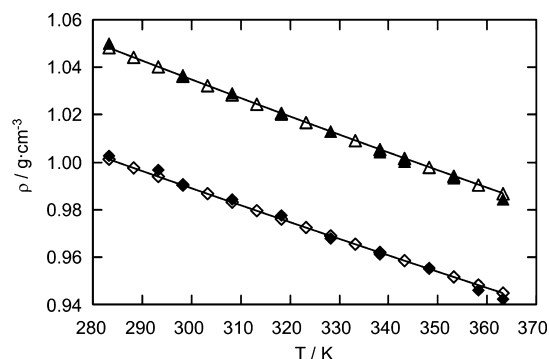
$$\rho = \rho_0 + \rho_1 T + \rho_2 T^2 \quad (4)$$

where all data are taken into account with the same statistical weight. In eq 4, the fit parameters for [HMIM][B(CN)<sub>4</sub>] were determined to be  $\rho_0 = 1.23711 \text{ g} \cdot \text{cm}^{-3}$ ,  $\rho_1 = -0.93216 \times 10^{-3} \text{ g} \cdot \text{cm}^{-3} \cdot \text{K}^{-1}$ , and  $\rho_2 = 3.52838 \times 10^{-7} \text{ g} \cdot \text{cm}^{-3} \cdot \text{K}^{-2}$ . The root-mean-square deviation of the experimental density data from the correlation according to eq 4 is 0.0004%, and the relative deviation of all single data points from the fit lies clearly within the measurement uncertainty of  $\pm 0.02\%$ .

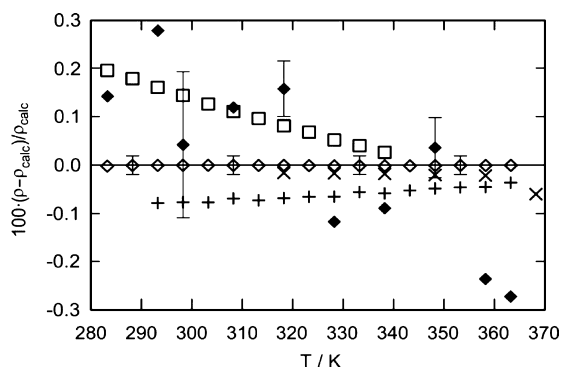
For the simulated results of [HMIM][B(CN)<sub>4</sub>], very good agreement with the density data measured by the U-tube densimeter was found, as shown in Figure 2. The deviation of the

**Table 3.** Liquid Density of [HMIM][B(CN)<sub>4</sub>] from Experiment ( $\rho_{\text{exp}}$ ) and Simulation ( $\rho_{\text{sim}}$ ) at Atmospheric Pressure

<i>T</i> (K)	$\rho_{\text{exp}}$ (g·cm <sup>−3</sup> )	$\rho_{\text{sim}}$ (g·cm <sup>−3</sup> )
283.15	1.00145	1.003 ± 0.001
288.15	0.99781	—
293.15	0.99417	0.997 ± 0.001
298.15	0.99056	0.991 ± 0.002
303.15	0.98696	—
308.15	0.98337	0.985 ± 0.001
313.15	0.97981	—
318.15	0.97626	0.978 ± 0.001
323.15	0.97273	—
328.15	0.96921	0.968 ± 0.001
333.15	0.96572	—
338.15	0.96224	0.961 ± 0.002
343.15	0.95878	—
348.15	0.95534	0.956 ± 0.001
353.15	0.95193	—
358.15	0.94852	0.946 ± 0.001
363.15	0.94513	0.943 ± 0.002

**Figure 2.** Liquid density  $\rho$  for ILs at atmospheric pressure as a function of temperature (—, eq 4). [HMIM][B(CN)<sub>4</sub>]:  $\diamond$ , this study, experiment;  $\blacklozenge$ , this study, simulation. [EMIM][B(CN)<sub>4</sub>]:  $\Delta$ , Koller et al., experiment;<sup>5</sup>  $\blacktriangle$ , Koller et al., simulation.<sup>4</sup>

MD calculations presented in Figure 3 is less than  $\pm 0.3\%$  from the experimental data according to eq 4, confirming an excellent prediction over a broad temperature range from 283.15 to 363.15 K. In the figure, error bars depict as examples the expanded

**Figure 3.** Comparison of liquid density data  $\rho$  for [HMIM][B(CN)<sub>4</sub>] at atmospheric pressure as a function of temperature (—, eq 4):  $\diamond$ , this study, experiment;  $\blacklozenge$ , this study, simulation; +, Mota-Martinez et al.;<sup>38</sup> ×, Domańska et al.;<sup>39</sup>  $\square$ , Tong et al.<sup>40</sup>

uncertainties ( $k = 2$ ) for our experiments and the statistical uncertainties of the simulations.

In our previous studies on [EMIM][B(CN)<sub>4</sub>],<sup>4,5</sup> the simulated density data also fitted the experimental values very well, with deviations in the same range as those for [HMIM][B(CN)<sub>4</sub>]. The excellent agreement for the density of [HMIM][B(CN)<sub>4</sub>] was obtained by the small adjustment of the LJ size parameters of the nitrogen atoms in the anion. In conclusion, our atomistic model partially transferred from [EMIM][B(CN)<sub>4</sub>] to the homologous IL [HMIM][B(CN)<sub>4</sub>] is capable of predicting reliable temperature-dependent data for the equilibrium property density, which is a first indication of the good quality of the FF.

In terms of the influence of the cation variation on the experimental density data, lower densities for [HMIM][B(CN)<sub>4</sub>] compared to [EMIM][B(CN)<sub>4</sub>] were found.<sup>5</sup> The deviation of the densities of [HMIM][B(CN)<sub>4</sub>] from those of [EMIM][B(CN)<sub>4</sub>] covers the range from  $-4.5\%$  at 283.15 K to  $-4.2\%$  at 363.15 K. The difference in density between the two homologous ILs containing the [B(CN)<sub>4</sub>]<sup>−</sup> anion can be explained by the different sizes of the associated cations, where the [HMIM]<sup>+</sup> cation is larger and contains a longer alkyl chain than the [EMIM]<sup>+</sup> cation. This structure results in less dense packing and, hence, a lower mass density for [HMIM][B(CN)<sub>4</sub>]. This is in agreement with investigations of other ILs containing 1-alkyl-3-methylimidazolium cations and the same anion, where decreasing densities with increasing alkyl-chain length were observed.<sup>5,13,15</sup> As already described for [EMIM][B(CN)<sub>4</sub>], the relatively low densities of ILs based on [B(CN)<sub>4</sub>]<sup>−</sup> compared to other ILs with comparable molar masses are mainly caused by the strong charge delocalization in the tetracyanoborate anion and, consequently, by its relatively weak coordination to the cation.<sup>5</sup>

Figure 3 also shows the deviations of our experimental densities and available literature data for [HMIM][B(CN)<sub>4</sub>] from eq 4. Mota-Martinez et al.<sup>38</sup> measured the density with an Anton Paar SVM 3000 viscosimeter claiming an uncertainty of  $\pm 0.0005$  g·cm<sup>−3</sup>, or approximately  $\pm 0.05\%$ . The deviations between their data and our data range from  $-0.08\%$  to  $-0.04\%$ , which is partially outside the combined estimated expanded uncertainties. The water content of less than 381 ppm measured by Mota-Martinez et al.<sup>38</sup> should not be the reason for the differences because it is very close to the water contents determined in our measurements. Different and/or undefined impurities might affect the measured density to that extent. Domańska et al.<sup>39</sup> used an Anton Paar 4500 vibrating-tube densimeter providing an automatic viscosity correction. Their specified uncertainty of less than  $5 \times 10^{-5}$  g·cm<sup>−3</sup> seems to be underestimated when taking into account both the error associated with the calibration and that of the subsequent measuring procedure. The data of Domańska et al.<sup>39</sup> correspond well with our values, with the deviations of about  $-0.02\%$  being within the combined estimated expanded uncertainties. Only the value at 368.15 K differs by  $-0.06\%$  with respect to our data correlation, which might be due to the fact that it is outside of the temperature range studied in our measurements.

In addition, Tong et al.<sup>40</sup> used a group contribution method to calculate the density of [HMIM][B(CN)<sub>4</sub>] as a function of temperature based on the measurements with a vibrating U-tube densimeter for [EMIM][B(CN)<sub>4</sub>]. The data of Tong et al.<sup>40</sup> are between  $+0.03\%$  and  $+0.20\%$  higher than our values and imply a different temperature dependence. No uncertainty was specified for the predicted values of [HMIM][B(CN)<sub>4</sub>]. For the measured data of [EMIM][B(CN)<sub>4</sub>], an uncertainty of  $1 \times 10^{-5}$  g·cm<sup>−3</sup>

was given, which is supposed to be underestimated for the densimeter used.

**Interfacial Tension.** Table 4 and Figure 4 summarize both experimental and simulated values obtained for the interfacial

**Table 4. Interfacial Tensions of [HMIM][B(CN)<sub>4</sub>] and [EMIM][B(CN)<sub>4</sub>] from Experiment ( $\sigma_{\text{exp}}$ ) and Simulation ( $\sigma_{\text{sim}}$ ) at Atmospheric Pressure**

<i>T</i> (K)	[HMIM][B(CN) <sub>4</sub> ]		[EMIM][B(CN) <sub>4</sub> ]
	$\sigma_{\text{exp}}$ (mN·m <sup>−1</sup> )	$\sigma_{\text{sim}}$ (mN·m <sup>−1</sup> )	$\sigma_{\text{sim}}$ (mN·m <sup>−1</sup> )
283.15	—	42.8 ± 2.0	47.5 ± 0.9
293.15	—	41.2 ± 1.5	46.0 ± 0.7
295.15	40.17 <sup>a</sup>	—	—
298.15	—	40.3 ± 1.2	45.8 ± 1.5
318.15	—	38.7 ± 1.6	43.6 ± 1.3
323.15	—	—	42.8 ± 1.4
338.15	—	36.6 ± 1.4	39.5 ± 0.8
343.15	33.53 <sup>b</sup>	36.1 ± 1.0	39.0 ± 1.4
353.15	32.58 <sup>b</sup>	—	—
358.15	—	33.9 ± 0.9	37.5 ± 0.8
363.15	30.89 <sup>b</sup>	33.2 ± 0.8	37.1 ± 0.9

<sup>a</sup>Pendant drop. <sup>b</sup>SLS.

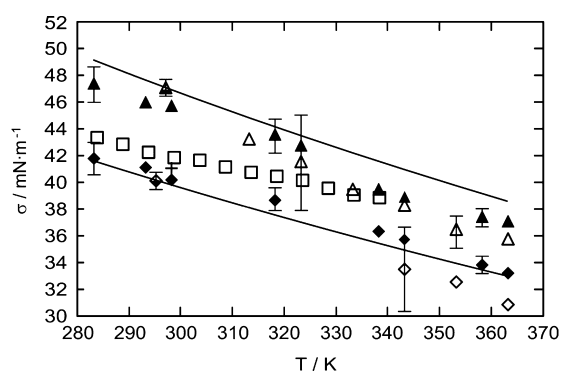


**Figure 4.** Comparison of surface tension data  $\sigma$  at atmospheric pressure as a function of temperature (—, eq 1). [HMIM][B(CN)<sub>4</sub>]:  $\diamond$ , this study, SLS; top-open diamond, this study, pendant drop;  $\blacklozenge$ , this study, simulation; +, Mota-Martinez et al.;<sup>38</sup>  $\square$ , Tong et al.<sup>40</sup> [EMIM][B(CN)<sub>4</sub>]:  $\blacktriangle$ , this study, simulation;  $\Delta$ , Koller et al., SLS;<sup>5</sup> top-open triangle, Koller et al., pendant drop.<sup>5</sup>

tension of [EMIM][B(CN)<sub>4</sub>] and [HMIM][B(CN)<sub>4</sub>]. For the latter, interfacial tension was determined from SLS experiments simultaneously with the viscosity in the temperature range from 343.15 to 363.15 K. Furthermore, a single datum was measured with the pendant drop technique at a temperature of 295.15 K at atmospheric pressure. From this value and the temperature dependence of density, the interfacial tension was predicted according to eq 1 in the temperature range from 283.15 to 333.15 K and used to evaluate the dynamic viscosity from the SLS experiments in the same temperature range. In Figure 4, error bars represent the estimated expanded uncertainties for both simulation and experiment.

Considering the experimental values for both ILs studied, the interfacial tension decreases with increasing temperature; see Figure 4. The predicted values are higher than the SLS data for both ILs. The correlation method and SLS data, however, seem to converge for low temperatures. As the prediction equation is mainly valid for high-viscosity fluids,<sup>20</sup> the increasing difference between the interfacial tension values at higher temperatures

might be due to the reduction of the viscosity to a range where the correlation cannot describe the true behavior anymore.

The simulated results are in good agreement with the experimental values both for the SLS results and for the prediction obtained from the pendant drop method. In the case of [HMIM][B(CN)<sub>4</sub>], deviations of the simulated values from the SLS data are less than +7.6%, which is in the range of the relatively large expanded uncertainty of the SLS results of  $\pm 8\%$ . The computed results deviate by between +1.3% and +3.4% from the prediction according to eq 1. For [EMIM][B(CN)<sub>4</sub>], comparisons of the simulation results with the SLS experiment and with the prediction method reveal an even better agreement, where differences from +1.7% to +3.7% and from −1.2% to −4.9%, respectively, can be found. The simulated and experimental values for both ILs are partially within the combined expanded uncertainties, demonstrating that the interfacial tension for both ILs can be captured well by our MD simulations for a broad temperature range. One reason for the existing discrepancy between simulation and experiment seems to be that corrections for the tail contributions of the long-range LJ interactions were determined assuming a homogeneous system with no density variations. Yet, density profiles are present in inhomogeneous IL–vacuum systems. With the corrections for energy and pressure used in this study,<sup>25</sup> the long-range corrections for the dispersion term in the LJ potential result in larger values in the interfacial tension. However, because of the large LJ cutoff used in our simulations, the effect of the long-range LJ interactions on the calculated data is assumed to be sufficiently taken into account. This is confirmed by calculations with larger cutoffs of 1.3 nm for [EMIM][B(CN)<sub>4</sub>] and 1.4 nm for [HMIM][B(CN)<sub>4</sub>], which implies extended computation times. For example state points over the complete temperature range, deviations from +1 to +3% from the results with a cutoff of 1.2 nm were found. These deviations are within the calculated statistical uncertainties of less than  $\pm 4\%$  for [EMIM][B(CN)<sub>4</sub>] and  $\pm 5\%$  for [HMIM][B(CN)<sub>4</sub>].

The interfacial tension values for [HMIM][B(CN)<sub>4</sub>] are smaller than those for [EMIM][B(CN)<sub>4</sub>]. For the SLS results, the deviation ranges from −10.8% to −13.7% related to the interfacial tension data of [EMIM][B(CN)<sub>4</sub>]. Moreover, a reduction of about 15% can be identified for the longer-chain IL [HMIM][B(CN)<sub>4</sub>] considering the predicted results obtained from the pendant drop method. In accordance with the findings of Law and Watson,<sup>41</sup> an increasing alkyl-chain length of the cation in the IL is associated with decreasing interfacial tension values. In agreement with our previous studies of different ILs based on the bis(trifluoromethylsulfonyl)imide ([NTf<sub>2</sub>]<sup>−</sup>) anion,<sup>13,15</sup> the higher molar volume of [HMIM][B(CN)<sub>4</sub>] compared to [EMIM][B(CN)<sub>4</sub>] results in a smaller interfacial tension. As explained by Tokuda et al.,<sup>42</sup> the relatively low interfacial tensions of the studied ILs based on [B(CN)<sub>4</sub>]<sup>−</sup> probably originate from the strong charge delocalization and thus low Lewis basicity of this anion having symmetrically distributed low negative charges.

A comparison of the data for [HMIM][B(CN)<sub>4</sub>] with experimental data from the literature is possible only for the results published by Mota-Martinez et al.<sup>38</sup> Applying the pendant drop technique at a single temperature of 298.15 K, they measured a value of 41.1 mN·m<sup>−1</sup> with an uncertainty of 0.3 mN·m<sup>−1</sup>; see Figure 4. The deviation of this datum from our prediction based on eq 1 is +3.2%, which is outside the estimated combined uncertainties. Similarly to the findings for the density of [HMIM][B(CN)<sub>4</sub>], the main reason for this discrepancy can



be found in the presence of other impurities rather than in the different water contents. Furthermore, results from a group contribution method reported by Tong et al.<sup>40</sup> are included in Figure 4. From the interfacial tension measured for [EMIM][B(CN)<sub>4</sub>] using a forced bubble tensiometer, they predicted data for different homologous ILs such as [HMIM][B(CN)<sub>4</sub>] without describing the exact method of calculating the values. Compared to the prediction based on our measurements with the pendant drop technique, the data of Tong et al.<sup>40</sup> in Figure 4 deviate by +4.3% at 283.15 K increasing to +9.7% at 338.15 K. The significantly larger values seem to stem from the data measured for [EMIM][B(CN)<sub>4</sub>], which were already more than 8% larger than those obtained by our SLS measurements.<sup>5</sup>

**Self-Diffusion Coefficient.** The experimental and simulated self-diffusion coefficients of the cation ( $D_+$ ) and anion ( $D_-$ ) for [HMIM][B(CN)<sub>4</sub>] are reported in Table 5. In Figure 5, these data are compared to the experimental and simulation results for [EMIM][B(CN)<sub>4</sub>] determined in our previous studies.<sup>4,5</sup>

**Table 5. Self-Diffusion Coefficients for the Cation and Anion of [HMIM][B(CN)<sub>4</sub>] from Experiment ( $D_{+,exp}$  and  $D_{-,exp}$ ) and Simulation ( $D_{+,sim}$  and  $D_{-,sim}$ ) at Atmospheric Pressure**

$T$ (K)	$D_{+,exp}$ ( $10^{-12} \text{ m}^2 \cdot \text{s}^{-1}$ )	$D_{-,exp}$ ( $10^{-12} \text{ m}^2 \cdot \text{s}^{-1}$ )	$D_{+,sim}$ ( $10^{-12} \text{ m}^2 \cdot \text{s}^{-1}$ )	$D_{-,sim}$ ( $10^{-12} \text{ m}^2 \cdot \text{s}^{-1}$ )
278.15	7.6	7.3	—	—
283.15	9.9	10.7	—	—
288.15	12.8	12.8	—	—
293.15	17.0	16.1	$13.8 \pm 0.7$	$12.9 \pm 1.1$
298.15	22.8	21.7	$19.2 \pm 2.0$	$18.6 \pm 1.3$
303.15	28.8	28.1	—	—
308.15	36.7	34.1	$29.4 \pm 2.7$	$29.0 \pm 4.1$
313.15	45.2	42.0	—	—
318.15	—	—	$42.0 \pm 8.3$	$39.1 \pm 7.5$
338.15	—	—	$104 \pm 18$	$82 \pm 16$
348.15	—	—	$129 \pm 21$	$118 \pm 19$
358.15	—	—	$183 \pm 25$	$149 \pm 23$
393.15	—	—	$563 \pm 75$	$523 \pm 65$

The experimental data are presented in form of an Arrhenius-type equation

$$D_{\pm} = D_{0,\pm} \exp\left(-\frac{E_{A,\pm}}{RT}\right) \quad (5)$$

where  $D_0$  is the pre-exponential factor,  $E_{A,\pm}$  represents the activation energies for the self-diffusion of the cation (+) and anion (-), and  $R$  is the molar gas constant. For both ILs, because of the linear behavior in the Arrhenius plot, the self-diffusion coefficients tend to increase exponentially with increasing temperature, which can be observed in both the experimental and simulation data.

Figure 5 also shows that the simulation results for [HMIM][B(CN)<sub>4</sub>] agree very well with the experimental data obtained from NMR spectroscopy. The deviations of the simulated results from the experimental data are in a range from -19.8% to -14.3%, where the expanded uncertainties for the simulations are less than  $\pm 20\%$  and those for the experiments are less than  $\pm 10\%$ . Similar results were found for [EMIM][B(CN)<sub>4</sub>].<sup>4,5</sup> In general, the simulations provide slightly lower values for all self-diffusion coefficient data than the experiments. This tendency is more pronounced for [HMIM][B(CN)<sub>4</sub>] than for [EMIM][B(CN)<sub>4</sub>]. The deviations might originate from different sources

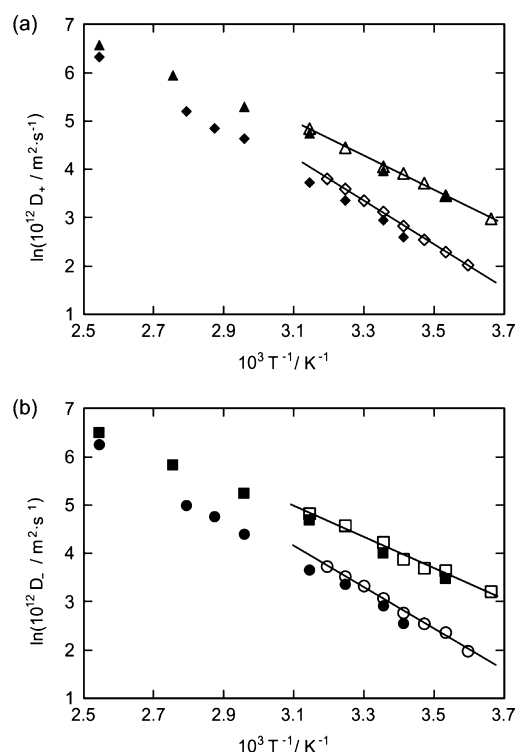


**Figure 5.** Self-diffusion coefficients  $D_{\pm}$  for IL (a) cations and (b) anions at atmospheric pressure as functions of temperature (—, eq 5). [HMIM][B(CN)<sub>4</sub>]:  $\diamond$ , [HMIM]<sup>+</sup>, this study, experiment;  $\circ$ , [B(CN)<sub>4</sub>]<sup>-</sup>, this study, experiment;  $\blacklozenge$ , [HMIM]<sup>+</sup>, this study, simulation;  $\bullet$ , [B(CN)<sub>4</sub>]<sup>-</sup>, this study, simulation. [EMIM][B(CN)<sub>4</sub>]:  $\Delta$ , [EMIM]<sup>+</sup>, Koller et al., experiment;<sup>5</sup>  $\square$ , [B(CN)<sub>4</sub>]<sup>-</sup>, Koller et al., experiment;<sup>5</sup>  $\blacktriangle$ , [EMIM]<sup>+</sup>, Koller et al., simulation;<sup>4</sup>  $\blacksquare$ , [B(CN)<sub>4</sub>]<sup>-</sup>, Koller et al., simulation.<sup>4</sup>

such as the applied UA approach and the FF parameters. The latter seem to be responsible for the larger deviations between simulation and experiment for the self-diffusion coefficients of [HMIM][B(CN)<sub>4</sub>]. For this IL, the transfer of the non-electrostatic FF optimized for [EMIM][B(CN)<sub>4</sub>] and the derivation of the electrostatic FF approximated by calculations for [BMIM][B(CN)<sub>4</sub>] are simplifications that can affect the calculated data, especially for transport properties. Nevertheless, all findings imply that the atomistic model transferred to [HMIM][B(CN)<sub>4</sub>] can provide self-diffusion coefficients for both ions consistent with experimental data, with statistical uncertainties in the same range as those for [EMIM][B(CN)<sub>4</sub>]. In addition, it should be emphasized that the good agreement for the self-diffusion coefficients for both ILs goes along with an excellent prediction of the density by the simulations.

In agreement with the experimental measurements, our MD simulations for both ILs produce self-diffusion coefficients for the cations that are about 10% higher than those for the anions over the complete temperature range, even though the cation is larger and heavier than the anion. This behavior can be attributed to a preferential movement of the cation parallel to the plane of the imidazolium ring. In this case, the long and bulky alkyl chains of the [EMIM]<sup>+</sup> and [HMIM]<sup>+</sup> cations are in the same plane as the imidazolium ring, which facilitates the motion of the cation in the direction within this plane. In contrast, the three-dimensional tetrahedral structure of the tetracyanoborate anion sterically hinders the diffusion in the bulk, even though its molecular weight is much smaller than that of the cations. Tokuda et



al.<sup>42–44</sup> have found the same trend for the self-diffusivity of the ions in different imidazolium-based ILs.

From the slope of the Arrhenius plots according to eq 5, activation energies for the self-diffusion from the experimental and simulated data were determined and are reported in Table 6.

**Table 6. Activation Energies for Self-Diffusion of Cations ( $E_{A,+}$ ) and Anions ( $E_{A,-}$ ) of ILs**

IL	method	$E_{A,+}$ (kJ·mol <sup>-1</sup> )	$E_{A,-}$ (kJ·mol <sup>-1</sup> )
[EMIM][B(CN) <sub>4</sub> ]	experiment	29.5	26.7
	simulation	26.4	25.4
[HMIM][B(CN) <sub>4</sub> ]	experiment	37.6	35.8
	simulation	35.0	33.8

Apparently, the simulated activation energies agree well with the experimental values for both ILs and deviate in the range from −5.2% to −10.5%. The good agreement of the simulated and experimental activation energies confirms the capability of the models to predict the temperature dependence of the self-diffusion coefficients for both ILs. From both methods, higher activation energies are found for [HMIM][B(CN)<sub>4</sub>] than for [EMIM][B(CN)<sub>4</sub>], as well as for the cation than for the anion.

From both the experimental and simulated data, it is found that the self-diffusion coefficients for both ions of [HMIM][B(CN)<sub>4</sub>] obtained in this work are distinctly smaller than those for [EMIM][B(CN)<sub>4</sub>]. In detail, the differences from the experiments cover the range from −68.9% at 283.15 K to −57.4% at 308.15 K for the cation and are even more pronounced for the anion, with values from −72.2% to −65.1% in the same temperature range. The reduced mobility of both ions for [HMIM][B(CN)<sub>4</sub>] seems to be dominated by the sterical influence of the longer alkyl chain with six carbon atoms hindering the self-diffusion of both the cation and the anion. In addition to this effect, the hexyl chain is capable of forming van der Waals (vdW) interactions, which might decrease the self-diffusion coefficients for both ions. For different [NTf<sub>2</sub>]<sup>−</sup>-based ILs with varying 1-alkyl-3-methylimidazolium cations, Tokuda et al.<sup>42</sup> also found that increasing the cationic alkyl-chain length implies smaller self-diffusion coefficients for both ions, except for [EMIM][NTf<sub>2</sub>] compared to the 1-methyl-3-methylimidazolium ([MMIM]<sup>+</sup>) homologue. As observed for [EMIM][B(CN)<sub>4</sub>] in our previous study,<sup>5</sup> the mentioned relatively weak interactions between the tetracyanoborate anion and the cation seem to contribute to the comparatively high self-diffusivity. Consequently, larger values can be found for both ions of [HMIM][B(CN)<sub>4</sub>] in comparison with the experimental results for other [HMIM]<sup>+</sup>-based ILs such as [HMIM][NTf<sub>2</sub>].<sup>42</sup> No further experimental and simulated data for the self-diffusion coefficients of [HMIM][B(CN)<sub>4</sub>] could be found in the literature.

**Viscosity.** The results for the dynamic viscosity,  $\eta$ , of [HMIM][B(CN)<sub>4</sub>] from SLS and MD simulation at temperatures between 283.15 and 363.15 K are reported in Table 7 and Figure 6. In the latter, results for [EMIM][B(CN)<sub>4</sub>] obtained from experiment and simulation are included for comparison.<sup>4,5</sup>

For the SLS measurements, each data point reflects the average of at least six independent measurements with different moduli of the wave vector  $q$ . To describe the temperature dependence, the experimental data for [HMIM][B(CN)<sub>4</sub>] can well be represented in the form of a Vogel equation

$$\eta = \eta_0 \exp[B/(T - C)] \quad (6)$$

**Table 7. Dynamic Viscosity of [HMIM][B(CN)<sub>4</sub>] from Experiment ( $\eta_{\text{exp}}$ ) and Simulation ( $\eta_{\text{sim}}$ ) at Atmospheric Pressure**

$T$ (K)	$\eta_{\text{exp}}$ (mPa·s)	$\eta_{\text{sim}}$ (mPa·s)
283.15	113.81	—
293.15	61.87	76.2 ± 9.4
298.15	—	54.2 ± 5.2
303.15	39.19	—
308.15	—	33.1 ± 5.3
313.15	24.87	29.0 ± 4.7
318.15	—	21.3 ± 2.2
323.15	16.64	—
328.15	—	14.7 ± 2.6
333.15	12.14	—
338.15	—	11.4 ± 1.5
343.15	8.65	—
348.15	—	8.2 ± 0.6
353.15	6.34	—
358.15	—	6.4 ± 0.9
363.15	4.59	5.5 ± 0.5

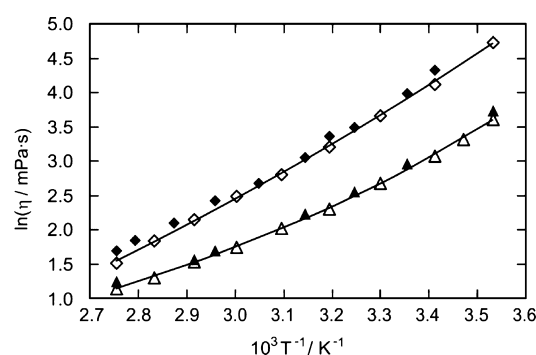


**Figure 6.** Dynamic viscosity,  $\eta$ , for ILs at atmospheric pressure as a function of temperature (—, eq 6). [HMIM][B(CN)<sub>4</sub>]:  $\diamond$ , this study, experiment;  $\blacklozenge$ , this study, simulation. [EMIM][B(CN)<sub>4</sub>]:  $\Delta$ , Koller et al., experiment;<sup>5</sup>  $\blacktriangle$ , Koller et al., simulation.<sup>4</sup>

where  $T$  is the temperature in Kelvin and  $\eta_0 = 0.00695$  mPa·s,  $B = 1602.029$  K, and  $C = 117.632$  K are the fit parameters. For the data correlation, the statistical weights of all data points are assumed to be the same. The root-mean-square deviation of the viscosity data from the fit is 2.3%. The relative deviation of most of the single data points from the fit according to eq 6 is smaller than the expanded uncertainty ( $k = 2$ ) of less than  $\pm 3\%$  for temperatures between 283.15 and 333.15 K and  $\pm 6\%$  in the transition range from 343.15 to 363.15 K.

As expected, the viscosity decreases with increasing temperatures for both ILs, as can be observed from both experiment and simulation; see Figure 6. In Figure 7, the deviations of the experimental and simulated data for [HMIM][B(CN)<sub>4</sub>] from the fit according to eq 6 are given, where the expanded uncertainties ( $k = 2$ ) of the results are shown as examples by error bars.

The viscosity is captured reasonably well by the simulations, with deviations ranging from +19.1% to +4.1% compared to the fit based on the experimental data. These deviations are only somewhat larger than those found for our computations performed for [EMIM][B(CN)<sub>4</sub>] in a previous study,<sup>4</sup> which verifies the good quality of the transferred MD model. In addition, the temperature dependence of the viscosity for [HMIM][B(CN)<sub>4</sub>] is reproduced satisfactorily by the simu-

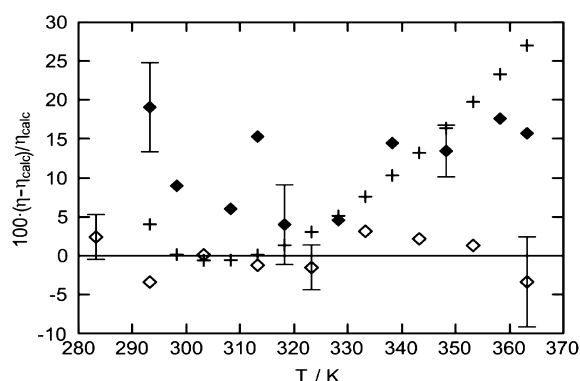


**Figure 7.** Comparison of dynamic viscosity data  $\eta$  for [HMIM][B(CN)<sub>4</sub>] at atmospheric pressure as a function of temperature (—, eq 6):  $\diamond$ , this study, experiment;  $\blacklozenge$ , this study, simulation; +, Mota-Martinez et al.<sup>38</sup>

lations. The slightly larger deviation of the computed results from the measured viscosity data for [HMIM][B(CN)<sub>4</sub>] is consistent with the findings for the self-diffusion coefficients and can be attributed to the same effects. It can be concluded that the dynamics of the ILs represented by viscosity and self-diffusion coefficients are well predicted by the MD simulations. The good agreement for viscosity and self-diffusion coefficients is probably the result of the development of the nonelectrostatic interaction parameters for [EMIM][B(CN)<sub>4</sub>] combined with the application of reduced total charges from the EA-RESP procedure. These calculated charges can be considered to be effective atomic partial charges accounting for the overall effects of the polarization in nonpolarizable FFs.

Our data obtained from experiment and simulation for the viscosity,  $\eta$ , and the self-diffusion coefficient,  $D$ , show a reciprocal behavior with respect to temperature. The generally known correlation for the two transport properties is the Stokes–Einstein equation

$$D = \frac{k_B T}{6\pi\eta r_{\text{eff}}} \quad (7)$$

where  $r_{\text{eff}}$  represents the effective hydrodynamic radius of a molecule and  $k_B$  is the Boltzmann constant. As explained by Liu et al.,<sup>45</sup> the relation is not appropriate for ILs because of their nonspherical nature. Hence, they suggested a fractional Stokes–Einstein equation of the form

$$D \propto (T\eta^{-1})^\beta \quad (8)$$

with  $\beta = 1$  for a Stokes–Einstein fluid. Equation 8 is applied for both ions of the ILs [EMIM][B(CN)<sub>4</sub>] and [HMIM][B(CN)<sub>4</sub>] in a double-logarithmic plot of  $D$  versus  $T\eta^{-1}$  for experiment and simulation in Figure 8.

From a linear fit of the data,  $\beta$  values ranging from 0.75 to 0.97 were obtained and are listed in Table 8. Here, the absolute uncertainties for  $\beta$  ( $k = 2$ ) resulting from the fitting procedures are also included.

Consistency of the results from experiment and simulation is found for [HMIM][B(CN)<sub>4</sub>]. The results for [EMIM][B(CN)<sub>4</sub>] agree within the combined experimental and simulation uncertainties. Our results are similar to those of Liu et al.<sup>45</sup> for different ILs, where mainly  $\beta$  values less than 1 were reported, for example, 0.94 and 0.95 for the cation and anion, respectively, of [BMIM][NTf<sub>2</sub>]. In agreement with previous simulation results,<sup>46,47</sup> our data confirm that the behavior of the studied

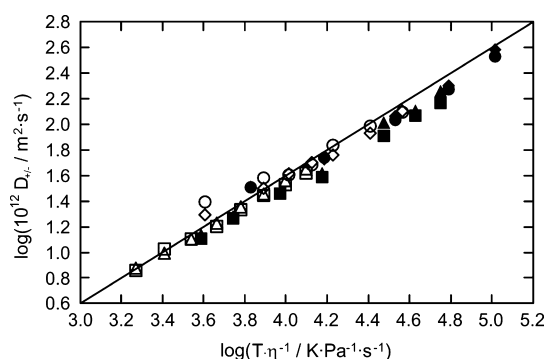


**Figure 8.** Double-logarithmic plot of  $D_{\pm}$  versus  $T\eta^{-1}$  for IL cations and anions (—, eq 8 with  $\beta = 1$ ). [HMIM][B(CN)<sub>4</sub>]:  $\diamond$ , [HMIM]<sup>+</sup>, this study, experiment;  $\circ$ , [B(CN)<sub>4</sub>]<sup>−</sup>, this study, experiment;  $\blacklozenge$ , [HMIM]<sup>+</sup>, this study, simulation;  $\bullet$ , [B(CN)<sub>4</sub>]<sup>−</sup>, this study, simulation. [EMIM][B(CN)<sub>4</sub>]:  $\Delta$ , [EMIM]<sup>+</sup>, Koller et al., experiment;<sup>5</sup>  $\square$ , [B(CN)<sub>4</sub>]<sup>−</sup>, Koller et al., experiment;<sup>5</sup>  $\blacktriangle$ , [EMIM]<sup>+</sup>, Koller et al., simulation;<sup>4</sup>  $\blacksquare$ , [B(CN)<sub>4</sub>]<sup>−</sup>, Koller et al., simulation.<sup>4</sup>

**Table 8.** Fractional Stokes–Einstein Coefficients of Cations ( $\beta_+$ ) and Anions ( $\beta_-$ ) of ILs

IL	method	$\beta_+$	$\beta_-$
[EMIM][B(CN) <sub>4</sub> ]	experiment	$0.83 \pm 0.06$	$0.75 \pm 0.11$
	simulation	$0.90 \pm 0.12$	$0.86 \pm 0.10$
[HMIM][B(CN) <sub>4</sub> ]	experiment	$0.95 \pm 0.06$	$0.91 \pm 0.06$
	simulation	$0.97 \pm 0.06$	$0.91 \pm 0.06$

ILs does not follow the Stokes–Einstein model, but is consistent with that of other molten salts.

The viscosity of [HMIM][B(CN)<sub>4</sub>] is higher than that of [EMIM][B(CN)<sub>4</sub>] over the whole temperature range studied. Based on the experimental results, the deviation is more than a factor of 3 at 283.15 K, whereas it is reduced to +23.8% at 363.15 K. In general, aside from the entanglement of the molecules, the viscosity of ILs is generally influenced by Coulomb forces, vdW interactions, and hydrogen bonding. For [HMIM][B(CN)<sub>4</sub>], the higher viscosity can be explained with the longer hexyl chain in the cation compared to the ethyl chain for [EMIM][B(CN)<sub>4</sub>], enhancing the attractive vdW forces. This is in agreement with the findings of Bonhôte et al.,<sup>48</sup> who observed high viscosities for ILs with cations having a weak side-chain mobility and a high molecular weight. Tokuda et al.<sup>42</sup> also reported that increasing cation alkyl-chain lengths for [NTf<sub>2</sub>]<sup>−</sup>-based ILs induce higher viscosity, with the exception of [EMIM][NTf<sub>2</sub>] compared to [MMIM][NTf<sub>2</sub>]. Regarding the influence of the anion, Bonhôte et al.<sup>48</sup> stated that charge delocalization within the anion weakens intermolecular hydrogen bonding with the cation, yielding lower viscosities if not overcompensated by vdW interactions. In this respect, [HMIM][B(CN)<sub>4</sub>] exhibits a lower viscosity than other [HMIM]<sup>+</sup>-based ILs such as [HMIM][NTf<sub>2</sub>],<sup>42</sup> apparently because of the strong charge delocalization and hence weak coordination of the [B(CN)<sub>4</sub>]<sup>−</sup> anion.

For [HMIM][B(CN)<sub>4</sub>], only Mota-Martinez et al.<sup>38</sup> provided viscosity data for the temperature range of 293.15–363.15 K in the literature. They used an Anton Paar SVM 3000 viscosimeter claiming an instrumental uncertainty of  $\pm 0.005$  mPa·s. In comparison with our data fitted with eq 6, the results of Mota-Martinez et al.<sup>38</sup> deviate by −0.5% at 303.15 K increasing to +27.0% at 363.15 K; see Figure 7. It seems that the increasing deviation for higher temperatures arises from the increasing difference between the measurement and calibration temper-

atures, which are assumed to be close to room-temperature conditions. A dominant influence of the water content on the different results can be excluded because the corresponding values are very similar. Taking into account the specified uncertainty of  $\pm 0.005$  mPa·s, however, this value seems to be strongly underestimated because, for the measured ILs, it would imply a relative uncertainty of about  $\pm 0.008\%$  at 293.15 K.

## CONCLUSIONS

The two homologous ILs [EMIM][B(CN)<sub>4</sub>] and [HMIM][B(CN)<sub>4</sub>] were investigated in terms of refractive index, density, surface tension, self-diffusion coefficients, and viscosity as a function of temperature. For the determination of these properties, experimental measurements and MD simulations were performed for the IL [HMIM][B(CN)<sub>4</sub>] in continuation of our previous studies on [EMIM][B(CN)<sub>4</sub>].<sup>4,5</sup> For the MD simulations of [HMIM][B(CN)<sub>4</sub>], the nonelectrostatic FF developed for [EMIM][B(CN)<sub>4</sub>] was transferred to the longer-chain IL. The electrostatic FF was modified by applying the EA-RESP procedure to account for the effect of the alkyl chain on the partial charges. To test the reliability of the MD simulations, accurate experimental data were obtained by conventional and SLS measurements. In general, the simulations for [HMIM][B(CN)<sub>4</sub>] agree well with the experimental data, indicating a certain transferability of the nonelectrostatic FF. For the density, the comparison of the experimental and simulation results for both ILs reveals very good agreement, with deviations of less than  $\pm 0.3\%$ . The simulation results for the interfacial tension obtained from the virial method are satisfactory, with deviations of less than  $\pm 8\%$  from the experimental values. In contrast to other MD simulation studies<sup>45,49,50</sup> partially reflecting the dynamics of transport processes too sluggish, the calculated self-diffusion coefficients and viscosities of both ILs agree well with the experimental data, with deviations of less than  $\pm 30\%$ . The influence of the longer alkyl chain of [HMIM][B(CN)<sub>4</sub>] on the thermophysical properties is represented by lower density, lower interfacial tension, lower self-diffusion coefficients, and higher viscosity than for [EMIM][B(CN)<sub>4</sub>], which is in agreement with other studies.

## ASSOCIATED CONTENT

### Supporting Information

MD simulation results for the mean square displacement as a function of the simulation time for both ions of [HMIM][B(CN)<sub>4</sub>] at temperatures of 293.15 and 318.15 K. This material is available free of charge via the Internet at <http://pubs.acs.org>.

## AUTHOR INFORMATION

### Corresponding Author

\*Tel.: +49-9131-85-29789. Fax: +49-9131-85-29901. E-mail: [apf@aot.uni-erlangen.de](mailto:apf@aot.uni-erlangen.de).

### Notes

The authors declare no competing financial interest.

## ACKNOWLEDGMENTS

This work was supported by the German Research Foundation (Deutsche Forschungsgemeinschaft, DFG) through funding for the Erlangen Graduate School in Advanced Optical Technologies (SAOT) within the German Excellence Initiative. In addition, financial support from the Seventh European Commission Framework Programme for Research and Technological Development for the project "Novel Ionic Liquid and

Supported Ionic Liquid Solvents for Reversible Capture of CO<sub>2</sub>" (IOLICAP Project 283077) is gratefully acknowledged. The authors thank the Secretaria General Adjunta de Informática del Consejo Superior de Investigaciones Científicas (SGAI-CESGA) and the Centro de Supercomputación de Galicia (CESGA) for CPU allocation time. J.R. acknowledges financial support through the Ramón y Cajal program, Contract RYC-2011-09585. The authors also thank Merck KGaA, Darmstadt, Germany, for providing a sample of [HMIM][B(CN)<sub>4</sub>].

## REFERENCES

- (1) Maginn, E. J. Molecular Simulation of Ionic Liquids: Current Status and Future Opportunities. *J. Phys.: Condens. Matter* **2009**, *21*, 373101-1–373101-17.
- (2) Wasserscheid, P.; Welton, T. *Ionic Liquids in Synthesis*, 2nd ed.; Wiley-VCH Verlag: Weinheim, Germany, 2007.
- (3) Allen, M. P.; Tildesley, D. J. *Computer Simulation of Liquids*; Oxford University Press: New York, 1987.
- (4) Koller, T.; Ramos, J.; Garrido, N. M.; Fröba, A. P.; Economou, I. G. Development of a United-Atom Force Field for 1-Ethyl-3-methylimidazolium Tetracyanoborate Ionic Liquid. *Mol. Phys.* **2012**, *110*, 1115–1126.
- (5) Koller, T.; Rausch, M. H.; Schulz, P. S.; Berger, M.; Wasserscheid, P.; Economou, I. G.; Leipertz, A.; Fröba, A. P. Viscosity, Interfacial Tension, Self-Diffusion Coefficient, Density, and Refractive Index of Ionic Liquid 1-Ethyl-3-methylimidazolium Tetracyanoborate as a Function of Temperature at Atmospheric Pressure. *J. Chem. Eng. Data* **2012**, *57*, 828–835.
- (6) Bernhardt, E.; Finze, M.; Willner, H. Eine Effiziente Synthese von Tetracyanoboraten durch Sinterprozesse. *Z. Anorg. Allg. Chem.* **2003**, *629*, 1229–1234.
- (7) Bernhardt, E.; Henkel, G.; Willner, H. Die Tetracyanoborate M[B(CN)<sub>4</sub>], M = [Bu<sub>4</sub>N]<sup>+</sup>, Ag<sup>+</sup>, K<sup>+</sup>. *Z. Anorg. Allg. Chem.* **2000**, *626*, 560–568.
- (8) Yan, P. F.; Yang, M.; Liu, X. M.; Wang, C.; Tan, Z. C.; Welz-Biermann, U. Activity Coefficients at Infinite Dilution of Organic Solutes in the Ionic Liquid 1-Ethyl-3-methylimidazolium Tetracyanoborate [EMIM][TCB] Using Gas–Liquid Chromatography. *J. Chem. Thermodyn.* **2010**, *42*, 817–822.
- (9) Kuang, D.; Wang, P.; Ito, S.; Zakeeruddin, S. M.; Grätzel, M. Stable Mesoscopic Dye-Sensitized Solar Cells Based on Tetracyanoborate Ionic Liquid Electrolyte. *J. Am. Chem. Soc.* **2006**, *128*, 7732–7733.
- (10) Kuang, D. B.; Cedric, K.; Henry, J. S.; Robin, H. B.; Shaik, M. Z.; Michael, G. A New Ion-Coordinating Ruthenium Sensitizer for Mesoscopic Dye-Sensitized Solar Cells. *Inorg. Chim. Acta* **2008**, *361*, 699–706.
- (11) Mahurin, S. M.; Lee, J. S.; Baker, G. A.; Luo, H.; Dai, S. Performance of Nitrile-Containing Anions in Task-Specific Ionic Liquids for Improved CO<sub>2</sub>/N<sub>2</sub> Separation. *J. Membr. Sci.* **2010**, *353*, 177–183.
- (12) Fröba, A. P. Simultane Bestimmung von Viskosität und Oberflächenspannung transparenter Fluide mittels Oberflächenlichtstreuung. Dr.-Ing. Thesis, Friedrich-Alexander-Universität Erlangen-Nürnberg, Erlangen, Germany, 2002.
- (13) Fröba, A. P.; Kremer, H.; Leipertz, A. Density, Refractive Index, Interfacial Tension, and Viscosity of Ionic Liquids [EMIM][EtSO<sub>4</sub>], [EMIM][NTf<sub>2</sub>], [EMIM][N(CN)<sub>2</sub>], and [OMA][NTf<sub>2</sub>] in Dependence on Temperature at Atmospheric Pressure. *J. Phys. Chem. B* **2008**, *112*, 12420–12430.
- (14) Fröba, A. P.; Leipertz, A. Accurate Determination of Liquid Viscosity and Surface Tension Using Surface Light Scattering (SLS): Toluene under Saturation Conditions between 260 and 380 K. *Int. J. Thermophys.* **2003**, *24*, 895–921.
- (15) Hasse, B.; Lehmann, J.; Assenbaum, D.; Wasserscheid, P.; Leipertz, A.; Fröba, A. P. Viscosity, Interfacial Tension, Density, and Refractive Index of Ionic Liquids [EMIM][MeSO<sub>3</sub>], [EMIM]-[MeOHPO<sub>2</sub>], [EMIM][O<sub>2</sub>CSO<sub>4</sub>], and [BBIM][NTf<sub>2</sub>] in Dependence



on Temperature at Atmospheric Pressure. *J. Chem. Eng. Data* **2009**, *54*, 2576–2583.

(16) Langevin, D. *Light Scattering by Liquid Surfaces and Complementary Techniques*; Marcel Dekker: New York, 1992.

(17) Levich, V. G. *Physicochemical Hydrodynamics*; Prentice Hall: Englewood Cliffs, NJ, 1962.

(18) Lucassen-Reynders, E. H.; Lucassen, J. Properties of Capillary Waves. *Adv. Colloid Interface Sci.* **1969**, *2*, 347–395.

(19) Price, W. S. Pulsed-Field Gradient Nuclear Magnetic Resonance as a Tool for Studying Translational Diffusion: Part 1. Basic Theory. *Concepts Magn. Reson.* **1997**, *9*, 299–336.

(20) MacLeod, D. B. On a Relation Between Surface Tension and Density. *Trans. Faraday Soc.* **1923**, *19*, 38–41.

(21) Sugden, S. The Variation of Surface Tension with Temperature and Some Related Functions. *J. Chem. Soc., Trans.* **1924**, *125*, 32–41.

(22) Fröba, A. P.; Leipertz, A. Viscosity of Diisodecyl Phthalate by Surface Light Scattering (SLS). *J. Chem. Eng. Data* **2007**, *52*, 1803–1810.

(23) Liu, Z.; Chen, T.; Bell, A. T.; Smit, B. Improved United-Atom Force Field for 1-Alkyl-3-methylimidazolium Chloride. *J. Phys. Chem. B* **2010**, *114*, 4572–4582.

(24) Cornell, W. D.; Cieplak, P.; Bayly, C. I.; Gould, I. R.; Merz, K. M., Jr.; Ferguson, D. M.; Spellmeyer, D. C.; Fox, T.; Caldwell, J. W.; Kollman, P. A. A Second Generation Force Field for the Simulation of Proteins, Nucleic Acids, and Organic Molecules. *J. Am. Chem. Soc.* **1995**, *117*, 5179–5197.

(25) Hess, B.; Kutzner, C.; van der Spoel, D.; Lindahl, E. GROMACS 4: Algorithms for Highly Efficient, Load-Balanced, and Scalable Molecular Simulation. *J. Chem. Theory Comput.* **2008**, *4*, 435–447.

(26) Hoover, W. G. Canonical Dynamics: Equilibrium Phase-Space Distributions. *Phys. Rev. A* **1985**, *31*, 1695–1697.

(27) Nosé, S. A Molecular Dynamics Method for Simulations in the Canonical Ensemble. *Mol. Phys.* **1984**, *52*, 255–268.

(28) Nosé, S.; Klein, M. L. Constant Pressure Molecular Dynamics for Molecular Systems. *Mol. Phys.* **1983**, *50*, 1055–1076.

(29) Parrinello, M.; Rahman, A. Polymorphic Transitions in Single Crystals: A New Molecular Dynamics Method. *J. Appl. Phys.* **1981**, *52*, 7182–7190.

(30) Essmann, U.; Perera, L.; Berkowitz, M. L.; Darden, T. A.; Lee, H.; Pedersen, L. G. A Smooth Particle Mesh Ewald Method. *J. Chem. Phys.* **1995**, *103*, 8577–8593.

(31) Frenkel, D.; Smit, B. *Understanding Molecular Simulation*, 1st ed.; Academic Press: New York, 1996.

(32) Bhargava, B. L.; Balasubramanian, S. Layering at an Ionic Liquid–Vapor Interface: A Molecular Dynamics Simulation Study of [bmim]–[PF<sub>6</sub>]. *J. Am. Chem. Soc.* **2006**, *128*, 10073–10078.

(33) González-Melchor, M.; Bresme, F.; Alejandre, J. Molecular Dynamics Simulations of the Surface Tension of Ionic Liquids. *J. Chem. Phys.* **2005**, *122*, 104710–104717.

(34) Rao, M.; Berne, B. J. On the Location of Surface of Tension in the Planar Interface between Liquid and Vapour. *Mol. Phys.* **1979**, *37*, 455–461.

(35) Vega, C.; de Miguel, E. Surface Tension of the Most Popular Models of Water by Using the Test-Area Simulation Method. *J. Chem. Phys.* **2007**, *126*, 154707-1–154707-10.

(36) Brocos, P.; Piñeiro, A.; Bravo, R.; Amigo, A. Refractive Indices, Molar Volumes and Molar Refractions of Binary Liquid Mixtures: Concepts and Correlations. *Phys. Chem. Chem. Phys.* **2003**, *5*, 550–557.

(37) Deetlefs, M.; Seddon, K. R.; Shara, M. Predicting Physical Properties of Ionic Liquids. *Phys. Chem. Chem. Phys.* **2006**, *8*, 642–649.

(38) Mota-Martinez, M. T.; Althuluth, M.; Kroon, M. C.; Peters, C. J. Solubility of Carbon Dioxide in the Low-Viscosity Ionic Liquid 1-Hexyl-3-methylimidazolium Tetracyanoborate. *Fluid Phase Equilib.* **2012**, *332*, 35–39.

(39) Domańska, U.; Vadimovna Lukoshko, E.; Wlazło, M. Measurements of Activity Coefficients at Infinite Dilution for Organic Solutes and Water in the Ionic Liquid 1-Hexyl-3-methylimidazolium Tetracyanoborate. *J. Chem. Thermodyn.* **2012**, *47*, 389–396.

(40) Tong, J.; Liu, Q.-S.; Kong, Y.-X.; Fang, D.-W.; Welz-Biermann, U.; Yang, J.-Z. Physicochemical Properties of an Ionic Liquid [C<sub>2</sub>mim][B-(CN)<sub>4</sub>]. *J. Chem. Eng. Data* **2010**, *55*, 3693–3696.

(41) Law, G.; Watson, P. R. Surface Tension Measurements of *n*-Alkylimidazolium Ionic Liquids. *Langmuir* **2001**, *17*, 6138–6141.

(42) Tokuda, H.; Hayamizu, K.; Ishii, K.; Susan, Md. A. B. H.; Watanabe, M. Physicochemical Properties and Structures of Room Temperature Ionic Liquids. 2. Variation of Alkyl Chain Length in Imidazolium Cation. *J. Phys. Chem. B* **2005**, *109*, 6103–6110.

(43) Tokuda, H.; Ishii, K.; Susan, Md. A. B. H.; Tsuzuki, S.; Hayamizu, K.; Watanabe, M. Physicochemical Properties and Structures of Room Temperature Ionic Liquids. 3. Variation of Cationic Structures. *J. Phys. Chem. B* **2006**, *110*, 2833–2839.

(44) Tokuda, H.; Hayamizu, K.; Ishii, K.; Susan, Md. A. B. H.; Watanabe, M. Physicochemical Properties and Structures of Room Temperature Ionic Liquids. 1. Variation of Anionic Species. *J. Phys. Chem. B* **2004**, *108*, 16593–16600.

(45) Liu, H.; Maginn, E. J.; Visser, A. E.; Bridges, N. J.; Fox, E. B. Thermal and Transport Properties of Six Ionic Liquids: An Experimental and Molecular Dynamics Study. *Ind. Eng. Chem. Res.* **2012**, *51*, 7242–7254.

(46) Köddermann, T.; Ludwig, R.; Paschek, D. On the Validity of Stokes–Einstein and Stokes–Einstein–Debye Relations in Ionic Liquids and Ionic-Liquid Mixtures. *ChemPhysChem* **2008**, *9*, 1851–1858.

(47) Spohr, H. V.; Patey, G. N. Structural and Dynamical Properties of Ionic Liquids: The Influence of Ion Size Disparity. *J. Chem. Phys.* **2008**, *129*, 064517-1–064517-8.

(48) Bonhôte, P.; Dias, A. P.; Papageorgiou, N.; Kalyanasundaram, K.; Grätzel, M. Hydrophobic, Highly Conductive Ambient-Temperature Molten Salts. *Inorg. Chem.* **1996**, *35*, 1168–1178.

(49) Andreussi, O.; Marzari, N. Transport Properties of Room-Temperature Ionic Liquids from Classical Molecular Dynamics. *J. Chem. Phys.* **2012**, *137*, 044508-1–044508-10.

(50) Liu, H.; Maginn, E. A Molecular Dynamics Investigation of the Structural and Dynamic Properties of the Ionic Liquid 1-*n*-Butyl-3-methylimidazolium Bis(trifluoromethanesulfonyl)imide. *J. Chem. Phys.* **2011**, *135*, 124507-1–124507-16.